

An adaptive spectral/DG method for a reduced phase-space based level set approach to geometrical optics on curved elements



Bernardo Cockburn^a, Chiu-Yen Kao^{b,*}, Fernando Reitich^a

^a School of Mathematics, University of Minnesota, Minneapolis, MN 55455, United States

^b Department of Mathematical Sciences, Claremont McKenna College, CA 91711, United States

ARTICLE INFO

Article history:

Received 14 August 2013

Received in revised form 4 December 2013

Accepted 8 December 2013

Available online 12 December 2013

Keywords:

Wave equation

Eikonal equation

Liouville equation

Geometrical optics

Level set method

Spectral method

Discontinuous Galerkin method

ABSTRACT

We present an adaptive spectral/discontinuous Galerkin (DG) method on curved elements to simulate high-frequency wavefronts within a reduced phase-space formulation of geometrical optics. Following recent work, the approach is based on the use of level sets defined by functions satisfying the Liouville equations in reduced phase-space and, in particular, it relies on the smoothness of these functions to represent them by rapidly convergent spectral expansions in the phase variables. The resulting (hyperbolic) system of equations for the coefficients in these expansions are then amenable to a high-order accurate treatment via DG approximations. In the present work, we significantly expand on the applicability and efficiency of the approach by incorporating mechanisms that allow for its use in scattering simulations and for a reduced overall computational cost. With regards to the former we demonstrate that the incorporation of curved elements is *necessary* to attain *any* kind of accuracy in calculations that involve scattering off non-flat interfaces. With regards to efficiency, on the other hand, we also show that the level-set formulation allows for a space p -adaptive scheme that under-resolves the level-set functions away from the wavefront without incurring in a loss of accuracy in the approximation of its location. As we show, these improvements enable simulations that are beyond the capabilities of previous implementations of these numerical procedures.

© 2013 Elsevier Inc. All rights reserved.

1. Introduction

In the absence of generally applicable numerical schemes that allow for full-wave calculations at very short wavelengths, the “geometrical optics” (GO) model [25] still constitutes the basis of state-of-the-art software tools for high-frequency wave simulations (see e.g. [1,18] and the references cited there). This model is derived from standard (acoustic, electromagnetic, elastic) wave equations via the WKB approximation procedure, resulting in an (“eikonal”) equation for the phase of the field

$$S_t(x, t) + c(x) |\nabla_x S(x, t)| = 0, \quad (1)$$

and in transport equations for the coefficients in an expansion of its amplitude in inverse powers of the wavenumber. The relevance of this model in a wide variety of applications (ranging from radar and imaging to path planning and control) has provided sustained impetus for the continued development of numerical techniques for its resolution. In this paper, we introduce a new approach that provides significant improvements over recently proposed techniques based on level-set

* Corresponding author.

E-mail addresses: cockburn@math.umn.edu (B. Cockburn), ckao@claremontmckenna.edu (C.-Y. Kao), reitich@math.umn.edu (F. Reitich).

formulations of the evolution of the wavefronts defined by Eq. (1) (that is, of the isosurfaces of the function S) when these are viewed as fronts in the extended phase-space.

The fully-nonlinear nature of Eq. (1) poses substantial challenges from both a theoretical and a computational perspective. Most importantly perhaps, and as is well-known, solutions are generally multi-valued. A single-valued solution can be distinguished in the viscosity sense which corresponds to waves of first arrival [9,10]. In a number of applications, however, knowledge of these waves is not sufficient, as waves with longer travel times may carry significant energy (possibly larger than that of first arrival; see e.g. [15]). In these cases, the standard approach to the numerical evaluation of multi-arrival travel times relies on Lagrangian “ray tracing”, that is, on the method of characteristics. In this context, this approach can be interpreted as following the evolution of particles under the Hamiltonian dynamics

$$\begin{cases} \frac{dx}{dt} = \nabla_p H(x, p) = c(x) \frac{p}{|p|}, \\ \frac{dp}{dt} = -\nabla_x H(x, p) = -|p| \nabla_x c(x), \end{cases} \tag{2}$$

where the Hamiltonian $H(x, p)$ is equal to $c(x)|p|$, and the position x and the momentum variable (or “slowness vector”) p constitute the “phase-space” (x, p) .

While certainly appealing due to its simplicity, the practical use of ray tracing may encounter substantial difficulties in the reconstruction of the wavefront, which must be effected through interpolation of points that evolve according to (2). More precisely, in cases where neighboring rays diverge from each other, the quality of the interpolated wavefront may quickly deteriorate unless additional tracking points (trajectories) are added a posteriori [20–22]. The need for simulation methodologies that can overcome these limitations and thus allow for more efficient and accurate representations, has generated a renewed interest in GO over the last few years; see e.g. [11] and the references therein. Among the resulting contributions, those that are based on solution of the Liouville equation

$$f_t(x, p, t) - \nabla_p f \cdot |p| \nabla_x c + \nabla_x f \cdot c(x) \frac{p}{|p|} = 0, \tag{3}$$

associated with (2) have been shown to hold significant promise [16,6,11,13,14,7]. This is largely due to the fact that (3) can be solved on an *Eulerian* (albeit higher-dimensional) grid thus avoiding issues of ray divergence. Moreover, the formulation in (3) can be interpreted as an “unfolding” of the multi-valued solutions of (1) and, as such, solutions to (3) are actually *smooth* in phase space.

Our approach is largely based on the developments in [7] which, in turn, relied on the level-set formulation of [16]. To introduce it, we first note that, since the Hamiltonian $H(x, p)$ remains constant along characteristics, it can be normalized to $H(x, p) = 1$, leading to the constraint

$$|p| = \frac{1}{c(x)}.$$

Thus, solutions to (3) can be sought in the form

$$f(x, p, t) = c(x) \delta(|p| - c(x)^{-1}) u\left(x, \frac{p}{|p|}, t\right).$$

In this paper, we shall consider two-dimensional wavefronts, in which case the above considerations allow for a recasting of Eq. (3) as

$$\mathcal{L}^2[u] = u_t + c \cos(\theta) u_{x_1} + c \sin(\theta) u_{x_2} + (c_{x_1} \sin(\theta) - c_{x_2} \cos(\theta)) u_\theta = 0, \tag{4}$$

where

$$x = (x_1, x_2), \quad p = c(x)^{-1} (\cos(\theta), \sin(\theta)),$$

and $u = u(x_1, x_2, \theta)$ is defined in the “reduced phase-space” (x, θ) . The formulation of [16] then is based on the observation that the wavefront can be defined as the intersection of level sets

$$\{u = 0\} \cap \{v = 0\},$$

of functions satisfying the linear (Liouville) equations

$$\begin{cases} \mathcal{L}^2[u] = 0, \\ \mathcal{L}^2[v] = 0. \end{cases} \tag{5}$$

The original approximate solutions of (5) in [16], however, relied on low-order finite-difference approximations (particularly at material interfaces) and thus they did not take full advantage of their smoothness. The work in [7], on the other

hand, sought to improve on this by introducing an entirely different approach to the discretization of the equations in (5). More precisely, this latter work proposed a spectral expansion of solutions in the phase variable θ (or phase variables (θ, ϕ) in three dimensions) and a high-order discontinuous Galerkin finite element approach to the solution of the hyperbolic system that results for the coefficients in the expansion. The initial developments in [7], however, were restricted to consideration of flat interfaces; and moreover, the approach entailed the detailed solution of the equations in (5) throughout their domain of definition, thus neglecting a significant characteristic of the model, namely, that only the evolution of the intersection of the zero level-sets of u and v is of interest.

In this paper, we propose means to overcome these two limitations. On the one hand, we show that the straightforward application of the scheme in [7] to simulations of scattering off curved surfaces fails to produce accurate solutions if the surface is not suitably approximated (see e.g. [3] for related observations in the context of CFD models). More importantly, we show that this can be remedied by introducing curved simplicial elements, and we detail how these can be implemented within the spectral/DG methodology. With regards to localization of solutions near the intersection of their zero isosurfaces, on the other hand, we introduce a space p -adaptive version of the algorithm that enables us to under-resolve away from the physical wavefront. For the present discussion, the adaptive mechanism is solely based on this qualitative localization principle, as we do not attempt to derive rigorous a-posteriori estimates that might provide more quantitative guidelines for a refinement strategy. Similarly, with regards to time-integration, we work with uniform time steps that lead to stable procedures in the presence of high-order discretizations. The derivation of a-posteriori estimates and of possible non-uniform time-stepping procedures are left for future work.

Even though we only applied our method to isotropic wave propagation, it can be extended to solve high frequency anisotropic wave propagation based on a similar framework proposed in [17].

The rest of the paper is organized as follows. First, and for the sake of completeness, we begin in the next section with a brief review of the spectral/DG formulation of [7], extending it to allow for curved simplicial elements. The specific elements are then described in Section 3, where we also explain our strategy for p -adaptivity. Numerical results obtained from an implementation of the resulting algorithms are included in Section 4, which substantiate our claims of improved applicability and efficiency without any sacrifice in accuracy. Finally, conclusions follow in Section 5.

2. A spectral/DG formulation

2.1. The spectral formulation in reduced phase-space

As we mentioned, the Liouville formulation (4) unfolds multi-valued solutions which thus become smooth in phase space. To take advantage of this property, we posit a spectral decomposition [7]

$$u(x_1, x_2, \theta, t) = \sum_{n=-N}^N U_n(x_1, x_2, t)e^{in\theta},$$

in the phase variables. From this, Eq. (4) readily implies that

$$U = \begin{bmatrix} U_{-N} \\ U_{-N+1} \\ \vdots \\ U_{N-1} \\ U_N \end{bmatrix} \in \mathbb{C}^{2N+1},$$

satisfies the linear system of equations

$$U_t + A_1 U_{x_1} + A_2 U_{x_2} + BU = 0, \tag{6}$$

where $A_1, A_2,$ and $B \in \mathbb{C}^{(2N+1) \times (2N+1)}$ are defined as

$$\begin{cases} (A_1)_{kl} = \frac{c}{2}\delta_{k-1,l} + \frac{c}{2}\delta_{k+1,l}, \\ (A_2)_{kl} = -\frac{ic}{2}\delta_{k-1,l} + \frac{ic}{2}\delta_{k+1,l}, \\ (B)_{kl} = -(N-i+2)\frac{\gamma}{2}\delta_{k-1,l} + (N-i)\frac{\gamma}{2}\delta_{k+1,l}. \end{cases}$$

Here

$$\delta_{k,l} = \begin{cases} 1 & \text{if } k=l, \\ 0 & \text{if } k \neq l, \end{cases}$$

denotes the Dirac delta,

$$\gamma = \gamma(x_1, x_2) = c_{x_1} + ic_{x_2},$$

and $\bar{\gamma} = c_{x_1} - ic_{x_2}$ denotes its conjugate.

2.2. The DG formulation in the space variables

The nature of the system (6) makes it amenable to a high-order treatment via discontinuous Galerkin (DG) discretizations [8]. To introduce these, we first rewrite the system in “conservation form”, that is, in the form

$$U_t + \text{div}(F(U)) + CU = 0, \tag{7}$$

where

$$F(U) = [A_1U, A_2U],$$

and $C = B - \partial_{x_1}A_1 - \partial_{x_2}A_2$, that is,

$$C = -(N - k + 3)\frac{\bar{\gamma}}{2}\delta_{k-1,l} + (N - k - 1)\frac{\gamma}{2}\delta_{k+1,l}.$$

As was shown in [7], the system can be explicitly diagonalized. More precisely, if

$$v = (v_1, v_2) = (\cos(\eta), \sin(\eta))$$

denotes a unit vector and

$$A(v) = v_1A_1 + v_2A_2 = \frac{c}{2}(\delta_{k-1,l}e^{-i\eta} + \delta_{k+1,l}e^{i\eta}),$$

then we have

$$\Lambda = S^{-1}AS,$$

where $S = PV$,

$$(V)_{kl} = \frac{1}{\sqrt{N+1}} \sin\left(\frac{kl\pi}{2(N+1)}\right),$$

and P and Λ are diagonal matrices with

$$P(\eta)_{jj} = e^{-ij\eta}, \quad (\Lambda)_{jj} = \lambda_j = c(x_1, x_2) \cos\left(\frac{j\pi}{2(N+1)}\right).$$

Since there are exactly N positive and N negative eigenvalues,

$$\lambda_1 > \lambda_2 > \dots > \lambda_N > \lambda_{N+1} = 0 > \lambda_{N+2} > \dots > \lambda_{2N+1},$$

the matrix A can be decomposed as

$$A = A^+ + A^- = S(\eta)\Lambda^+(x_1, x_2)S^{-1}(\eta) + S(\eta)\Lambda^-(x_1, x_2)S^{-1}(\eta),$$

where

$$A^\pm = S(\eta)\Lambda^\pm(x_1, x_2)S^{-1}(\eta),$$

and $\Lambda^+ = \text{diag}(\lambda_1, \lambda_2, \dots, \lambda_N, 0, \dots, 0)$ and $\Lambda^- = \text{diag}(0, \dots, 0, \lambda_{N+2}, \dots, \lambda_{2N+1})$.

To approximate the solution of (7), we consider a curved simplicial partition $T_h = \{K_n\}$ of a computational domain $\Omega \in \mathbb{R}^2$ and local spaces $P^k(K_n)$ on each element K_n consisting of polynomials of degree smaller than or equal to k . Then, expanding

$$U_h|_{K_n} = \sum_{j=1}^{N_k} \phi_j(x_1, x_2)c_j^{K_n}(t) \tag{8}$$

in terms of basis functions $\phi_j \in P^k(K)$ (see Appendix A), a DG formulation takes on the form

$$\int_{K_n} \frac{\partial U_h}{\partial t} \phi \, dx - \int_{K_n} F(U_h) \cdot \nabla \phi \, dx + \int_{K_n} CU_h \phi \, dx + \int_{\partial K_n} \hat{F}_h \cdot \nu \phi \, ds = 0, \tag{9}$$

for all $\phi \in P^k(K_n)$, where ν is the outward unit normal vector to ∂K_n and $\widehat{F}_h \cdot \nu$ is the numerical flux on ∂K_n [8]. Letting $\phi = \phi_i$, Eq. (9) implies

$$\int_{K_n} \sum_{j=1}^{N_k} (c_j^{K_n}(t))_t \phi_j \phi_i \, dx_1 \, dx_2 - \int_{K_n} A_1 \sum_{j=1}^{N_k} c_j^{K_n}(t) \phi_j (\phi_i)_{x_1} \, dx_1 \, dx_2 - \int_{K_n} A_2 \sum_{j=1}^{N_k} c_j^{K_n}(t) \phi_j (\phi_i)_{x_2} \, dx_1 \, dx_2 + \int_{K_n} C \sum_{j=1}^{N_h} c_j^{K_n}(t) \phi_j \phi_i \, dx_1 \, dx_2 + \int_{\partial K_n} \widehat{F}_h \cdot \nu \phi_i \, ds = 0, \tag{10}$$

which defines a system of ordinary differential equations for $c_j^{K_n}(t)$ once an approximation to the flux is chosen. For the hyperbolic system (7), a most natural choice is that associated with “upwinding” which, with the above notation, corresponds to

$$\widehat{F}_h \cdot \nu = A^+ U_h^+ + A^- U_h^-,$$

where $U_h^\pm = \lim_{\epsilon \rightarrow 0} U_h(x \mp \epsilon \nu)$. Explicitly, we have

$$\widehat{F}_h \cdot \nu = A^+ \left(\sum_{j=1}^{N_k} \phi_j(x_1, x_2) c_j^{K_n}(t) \right)^+ + A^- \left(\sum_{j=1}^{N_k} \phi_j(x_1, x_2) c_j^{K_n}(t) \right)^-, \tag{11}$$

and, if $\partial K_{n1}, \partial K_{n2}, \partial K_{n3}$ denote the (curved) edges of K_n , we may write

$$\int_{\partial K_n} \widehat{F}_h \cdot \nu \phi_i \, ds = \sum_{f=1}^3 \sum_{j=1}^{N_k} \int_{\partial K_{nf}} (A^+ \phi_j c_j^{K_n}(t) + A^- \phi_j c_j^{neighbor(K_n)}(t)) \phi_i \, dl,$$

where $neighbor(K_n)$ is the simplex that shares the boundary ∂K_{nf} with K_n .

3. The adaptive method on curved elements

In this section, we describe in detail the procedure described in Section 2. To this end, we begin in Section 3.1 by describing the isoparametric elements we use for a higher order representation of the boundary $\partial\Omega$ which, as we shall see, allow for the application of the resulting scheme to the simulation of scattering off non-flat interfaces. In Section 3.2, on the other hand, we briefly describe our adaptivity strategy to reduce the overall computational effort.

3.1. Curved elements

To allow for general curved geometries, we use regular meshes of triangles (that is meshes whose triangles are such that the ratio of their diameter to the radius of the biggest ball totally included in them is uniformly bounded) and modify those with vertices on the curved boundaries by using standard isoparametric mappings; see, for example, [4,2].

We recall that these are elements wherein the basis for the mapping from a reference element $K_{ref} = \{(r, s) \in [-1, 1] \times [-1, 1], r + s \leq 1\}$ onto a general curved triangle coincides with the collection of local shape functions.

A general, isoparametric curved triangle K with vertices P_1, P_2, P_3 is defined as $K := \Psi(K_{ref})$, where

$$\Psi = \sum_{j=1}^{\frac{(p+1)(p+2)}{2}} d_j \psi_j : K_{ref} \rightarrow \mathbb{R}^2.$$

Here, ψ_j are basis functions of polynomials of total degree p and the coefficients d_j can be determined by requiring that Ψ interpolate $\frac{(p+1)(p+2)}{2}$, suitably defined collocation points.

More precisely, for instance, the geometry of a quadratic isoparametric element K with vertices P_1, P_2, P_3 is defined as $\Psi(K_{ref}) = K$ through the mapping

$$\Psi = \sum_{j=1}^6 d_j \psi_j : K_{ref} \rightarrow \mathbb{R}^2,$$

where

$$\begin{aligned} \psi_1(r, s) &= -(r + s)/2, & \psi_2(r, s) &= (r + 1)/2, \\ \psi_3(r, s) &= (s + 1)/2, & \psi_4(r, s) &= -(r + 1)(r + s), \\ \psi_5(r, s) &= (r + 1)(s + 1), & \psi_6(r, s) &= -(s + 1)(r + s). \end{aligned}$$

The coefficients $d_1, d_2, \dots, d_6 \in \mathbb{R}^2$ can be determined from the requirement that Ψ interpolate the vertices of K and points along its edges. Specifically, if $C = P_{j+3}$ is a given point on the edge joining $A = P_j$ and $B = P_{\text{mod}(j,3)+1}$ ($j = 1, 2, 3$), so that the image of

$$\Phi_E : [-1, 1] \rightarrow \mathbb{R}^2, \quad t \rightarrow A \frac{1-t}{2} + B \frac{1+t}{2} + \left(C - \frac{A+B}{2} \right) (1-t)(1+t),$$

defines the edge itself, we have

$$d_j = P_j, \quad d_{j+3} = P_{j+3} - (P_j + P_{\text{mod}(j,3)+1})/2.$$

With this notation, and transforming onto the reference triangle, Eq. (10) becomes

$$\begin{aligned} & \sum_{j=1}^{N_k} \int_{K_{\text{ref}}} \phi_i \phi_j J_{K_n} dr ds (c_j^{K_n}(t))_t \\ &= \sum_{j=1}^{N_k} \int_{K_{\text{ref}}} J_{K_n} (A_1 \phi_j ((\phi_i)_r r_y + (\phi_i)_s s_y)) dr ds c_j^{K_n}(t) + \sum_{j=1}^{N_k} \int_{K_{\text{ref}}} J_{K_n} (A_2 \phi_j ((\phi_i)_r r_y + (\phi_i)_s s_y)) dr ds c_j^{K_n}(t) \\ & \quad - \sum_{j=1}^{N_k} \int_{K_{\text{ref}}} C \phi_i \phi_j J_{K_n} dr ds c_j^{K_n}(t) - \sum_{f=1}^3 \sum_{j=1}^{N_k} \int_{-1}^1 (A^+ \phi_j c_j^{K_n}(t) + A^- \phi_j c_j^{\text{neighbour}(K_n)}(t)) \phi_i \|\Phi'_E(l)\| dl, \end{aligned} \tag{12}$$

where

$$J_{K_n} = |\det D\Psi(r, s)|.$$

Equivalently, letting

$$M_{ij}^{K_n} = \int_{K_{\text{ref}}} \phi_i \phi_j J_{K_n} dr ds, \tag{13}$$

$$D_{ij}^{A_1 r} = \int_{K_{\text{ref}}} J_{K_n} A_1 \phi_j (\phi_i)_r r_x dr ds, \quad D_{ij}^{A_2 r} = \int_{K_{\text{ref}}} J_{K_n} A_2 \phi_j (\phi_i)_r r_y dr ds, \tag{14}$$

$$D_{nm}^{A_1 s} = \int_{K_{\text{ref}}} J_{K_n} A_1 \phi_j (\phi_i)_s s_x dr ds, \quad D_{nm}^{A_2 s} = \int_{K_{\text{ref}}} J_{K_n} A_2 \phi_j (\phi_i)_s s_y dr ds, \tag{15}$$

$$\tilde{C}_{ij} = \int_{K_{\text{ref}}} C \phi_i \phi_j J_{K_n} dr ds,$$

the system to be solved takes the form

$$\begin{aligned} \sum_{j=1}^{N_k} M_{ij}^{K_n} (c_j^{K_n}(t))_t &= \sum_{j=1}^{N_k} (D_{ij}^{A_1 r} + D_{ij}^{A_1 s} + D_{ij}^{A_2 r} + D_{ij}^{A_2 s} - \tilde{C}_{ij}) c_j^{K_n}(t) - \sum_{f=1}^3 \sum_{j=1}^{N_k} \int_{-1}^1 (A^+ \phi_j c_j^{K_n}(t)) \phi_i \|\Phi'_E(l)\| dl \\ & \quad - \sum_{f=1}^3 \sum_{j=1}^{N_k} \int_{-1}^1 (A^- \phi_j c_j^{\text{neighbour}(K_n)}(t)) \phi_i \|\Phi'_E(l)\| dl. \end{aligned} \tag{16}$$

3.2. Adaptivity

Although the formulation (16) assumes a constant element order throughout the computational domain this is certainly not necessary to derive a well-posed scheme. This is particularly relevant in the present context where only the one-dimensional wavefront in the three-dimensional space (x_1, x_2, θ) is of interest. The wavefront is defined as the intersection of the zero level sets of

$$u(x_1, x_2, \theta, t) = \sum_{n=-N}^N U_n(x_1, x_2, t) e^{in\theta} = \sum_{n=-N}^N \sum_{j=1}^{N_k} \phi_j(x_1, x_2) c_{uj}^{K_n}(t) e^{in\theta},$$

and

$$v(x_1, x_2, \theta, t) = \sum_{n=-N}^N V_n(x_1, x_2, t) e^{in\theta} = \sum_{n=-N}^N \sum_{j=1}^{N_k} \phi_j(x_1, x_2) c_{vj}^{K_n}(t) e^{in\theta},$$

and this can be used to formalize an adaptive scheme wherein higher resolution is constrained to the vicinity of this intersection. Specifically, in this initial contribution, we propose a simple adaptive procedure that is based on the use of high-order elements only where the absolute values of u and v lie below a threshold h_c . More precisely, if

$$|u|, |v| < h_c,$$

at one of the vertices of K_n then we use a high-order $k = k_{high}$ there; otherwise, a lower order $k = k_{low}$ is used. As we mentioned, the study of possible improvements of this strategy based on rigorous a-posteriori estimates will be the subject of future work.

4. Numerical results

In this section, we present a variety of numerical results from an implementation of the procedure delineated in Section 3.1 that clearly demonstrate the improvements in applicability and efficiency over prior realizations. To complete the description of our present scheme to resolve the system (16), we need only specify the choice of basis functions, quadrature formulas and time integrator. For the latter we simply resort to “strong stability preserving Runge–Kutta (SSP-RK) methods” [12,5] of an order that is commensurate with that of the (highest-order) spatial elements, leading to a CFL condition

$$\Delta t \leq \frac{h}{2k_{high} + 1},$$

where h is minimum length of the edges; as we said, the exploration of alternative (adaptive) time stepping algorithms is left for future work. The (orthonormal) basis functions, derived from Jacobi polynomials, and the quadrature formulas we use [24], on the other hand, are described in Appendix A.

The numerical results that follow are intended to exemplify the convergence of the procedure, the effects of curved geometries, and those of p -adaptivity. For the sake of definiteness we shall consider interfaces that are “perfectly reflecting” although other boundary conditions can be treated with similar ease [7]. In the case of reflecting interfaces, the appropriate boundary condition translates to [7]

$$U_h^- = -S^-(BS^-)^{-1} B(I - \Pi^-)U_h^+,$$

where

$$(B)_{kl} = \delta_{k,l} - e^{i(2\eta - \pi)(N - (k-1))} \delta_{k, 2N+2-l},$$

η denotes the polar angle of the (exterior) normal vector at $x \in \partial\Omega$, and

$$\Pi^- = S^-(S^-)^T.$$

First, we test the accuracy of different order schemes. Since it is not trivial to have an exact solution of (4) satisfying the reflecting boundary condition, we test the convergence on the function

$$u(x, \theta, t) = (x^7 + y^7 - t^7) \sum_{k=-5}^5 e^{i4k\theta},$$

satisfying the inhomogeneous equation

$$u_t + c \cos(\theta)u_{x_1} + c \sin(\theta)u_{x_2} + (c_{x_1} \sin(\theta) - c_{x_2} \cos(\theta))u_\theta = G(x, \theta, t), \tag{17}$$

Table 1

Convergence test results at $T = 1$ for k -order approximation in space and $(k + 1)$ -order RK in time for $k = 1, 2, 3$ and 4. We successively partition the domain $[-1, 1] \times [-1, 1]$ into 2, 8, 32, 128, 512, 2014 triangular elements. The time step is also chosen such that the CFL condition is satisfied.

$N = 21$			$N = 21$		
RK 2			RK 3		
Triangles	L2-error	Order	Triangles	L2-error	Order
2	3.0907E+00		2	2.1048E+00	
8	1.9292E+00	0.68	8	7.7342E-01	1.44
32	9.4741E-01	1.03	32	1.9650E-01	1.98
128	3.2993E-01	1.52	128	3.2803E-02	2.58
512	9.2968E-02	1.82	512	4.6514E-03	2.81
2048	2.3892E-02	1.96	2048	5.4549E-04	3.09
8192	6.0038E-03	1.99			

$N = 21$			$N = 21$		
RK 4			RK 5		
Triangles	L2-error	Order	Triangles	L2-error	Order
2	8.6365E-01		2	6.6447E-01	
8	3.1817E-01	1.44	8	7.1111E-02	3.22
32	3.8033E-02	3.06	32	3.6080E-03	4.30
128	2.8857E-03	3.72	128	1.2810E-04	4.82
512	1.9952E-04	3.85	512	3.9567E-06	5.02
2048	1.1272E-05	4.15			

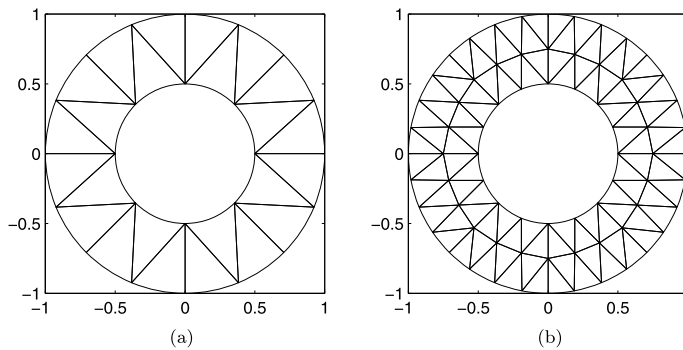


Fig. 1. The mesh with quadratic isoparametric elements for annulus with (a) 24 elements, (b) 96 elements.

for an appropriately defined function G and $c(x_1, x_2) = 1$ on the domain $\Omega = [-1, 1] \times [-1, 1]$. The specific form of the dependence of u on θ guarantees that it satisfies the boundary condition and also leads to a finite-term series in phase space. In Table 1, we show the convergence test for a DG formulation with polynomials of degree k and SSP-RK of degree $k + 1$. The results at $T = 1$ for $k = 1, 2, 3, 4$ are demonstrated on different number of triangular elements and global convergence in $k + 1$ order are observed.

Next, we test the accuracy of different order schemes on the mesh with curved elements. For simplicity, quadratic isoparametric elements are used. We use the function

$$u(x, \theta, t) = \sin(\pi t) \cos(\theta) \cos\left(2 \tan^{-1}\left(\frac{y}{x}\right) - \theta\right) = \sin(\pi t) \cos(\theta) \left(\frac{x^2 - y^2}{x^2 + y^2} \cos(\theta) + \frac{2xy}{x^2 + y^2} \sin(\theta)\right)$$

which satisfies the inhomogeneous equation (17) for an appropriately defined function G and $c(x_1, x_2) = 1$ on the annulus domain $\Omega = \{0.5 \leq r \leq 1\}$. Notice that this function satisfies the boundary conditions. The coarser mesh has 24 curved elements and is shown in Fig. 1(a), and its corresponding refined mesh is shown in Fig. 1(b). In Table 2, we show the convergence test for a DG formulation with polynomials of degree k and SSP-RK of degree $k + 1$. The results at $T = 0.5$ for $k = 1$ and 2 are demonstrated on different number of curved elements and global convergence in $k + 1$ order are also observed. With the usage of quadratic isoparametric elements, we observe the third order accuracy.

As mentioned before, curved elements can give a better representation of the geometry of the boundary. Here we would like to illustrate the fact that curved elements are crucial and need to be used when waves are reflected from the boundaries. This is mainly because we expect the solution to be smooth in the variable θ . If the boundary is not smooth, the boundary conditions may introduce spurious results.

We consider a seed point right at the focus $(0, 0)$ of a parabola $y = x^2 - \frac{1}{4}$. The boundary at $y = 0.75$ and the parabola $y = x^2 - \frac{1}{4}$ are reflecting boundaries. In Fig. 2(a), we sample points on the parabola to construct a triangulation of the domain. On the other hand, we use curved simplicial elements in Fig. 2(b). Numerical results for wavefronts with speed $c(x) = 1$ at $t = 0.1625, 0.325, 0.4875, 0.65, 0.8125, 0.975,$ and 1.1375 are shown in blue, green, red, cyan, magenta, yellow and blue respectively for both cases in the physical space. Since the seed point is right at the focus of parabola, the

Table 2

Convergence test results at $T = 0.5$ for difference order approximation in space and time. We successively partition the annulus domain $\Omega = \{0.5 \leq r \leq 1\}$ into 24, 96, 384, 1536, and 6144 curved elements.

$N = 21$			$N = 21$		
Triangles	RK 2	Order	Triangles	RK 3	Order
24	4.3455E-02		24	7.7779E-02	
96	1.1660E-02	1.90	96	1.1186E-03	2.80
384	3.0397E-03	1.94	384	1.5036E-04	2.89
1536	7.6903E-04	2.00	1536	1.9255E-05	2.97
6144	1.9356E-04	1.99	6144	2.4110E-06	3.00

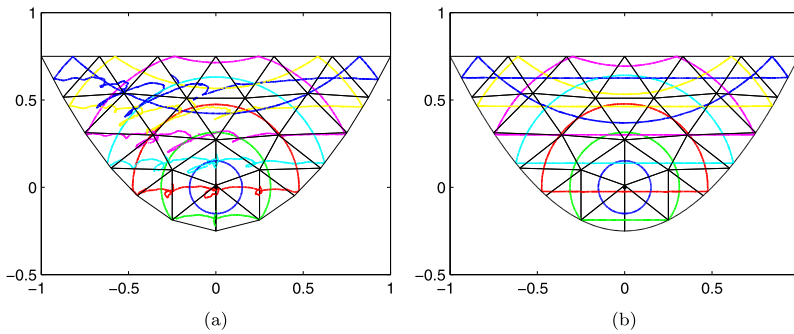


Fig. 2. The wavefronts with speed $c(x) = 1$ at $t = 0.1625, 0.325, 0.4875, 0.65, 0.8125$ and 0.975 for (a) regular triangular elements, (b) curved simplicial elements. (For interpretation of the colors in this figure, the reader is referred to the web version of this article.)

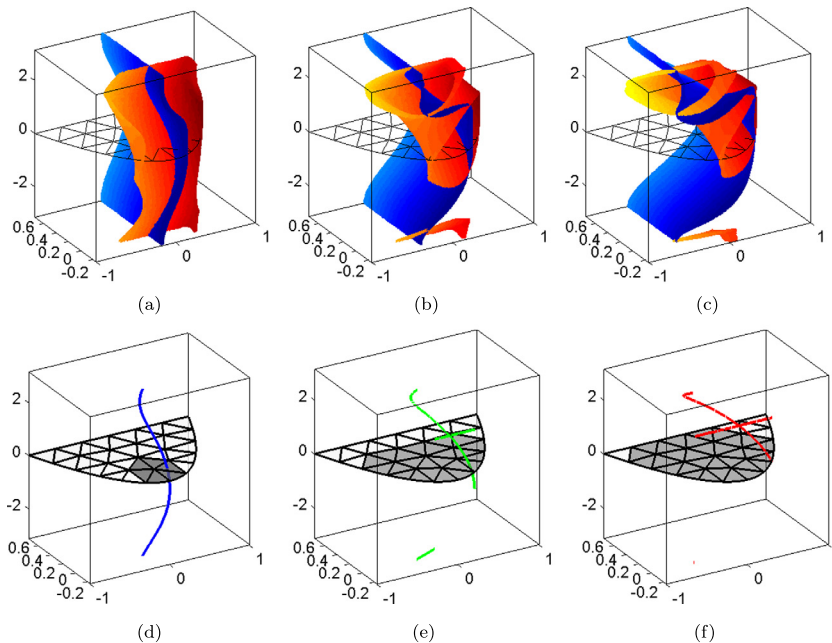


Fig. 3. (a) The zeros level sets at $t = 0.1625$. (b) The zeros level sets at $t = 0.325$. (c) The zeros level sets at $t = 0.4875$. (d) The wavefront in phase space at $t = 0.1625$. (e) The wavefront in phase space at $t = 0.325$. (f) The wavefront in phase space at $t = 0.4875$.

wavefronts reflected from the parabola boundary become plane wavefronts. We can see that the result on regular triangular elements display spurious oscillations while the result on curved elements are free of them and give a correct approximation to the exact solution.

Let us recall that these physical wavefronts are the projection of wavefronts in phase space. In Fig. 3(a, b, c), two zero level sets intersected with each other at the wavefront in phase space in Fig. 3(d, e, f) at $t = 0.1625, 0.325,$ and 0.4875 are shown. The level sets of u and v become convoluted as time involves. We see that one of the zero level set starts to wrap around itself and becomes tube-like. In Fig. 3(d, e, f), we also show the p -adaptivity mesh. High order $k_{high} = 4$

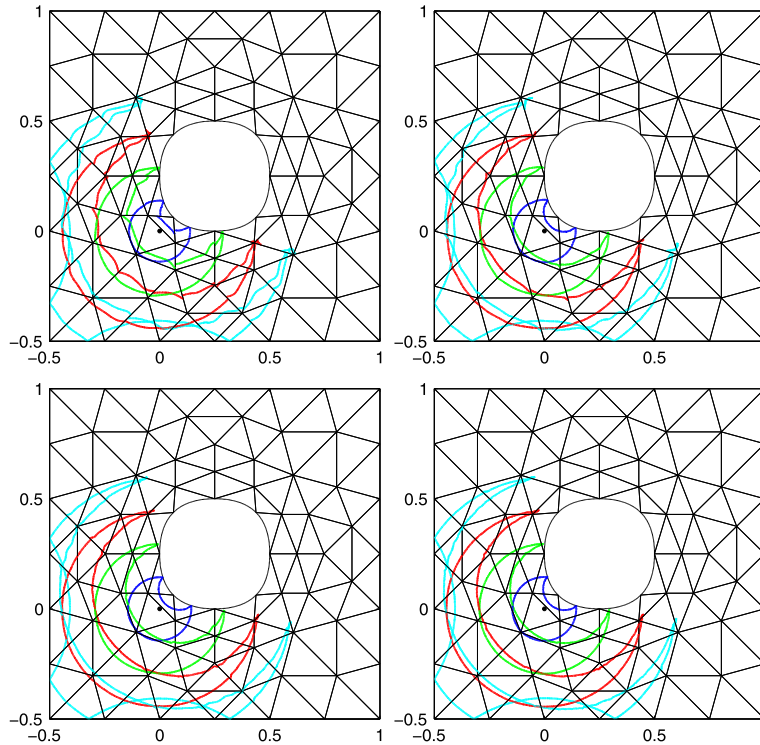


Fig. 4. The wavefront reflected from curved boundary at $t = 0.15, 0.3, 0.45$, and 0.6 for different order approximation in space and time with $k = 2$ (top, left), $k = 3$ (top, right), $k = 4$ (bottom, left) and $k = 5$ (bottom, right).

Table 3

Time comparison in seconds for non- p -adaptivity and p -adaptivity method at various time with $p = 2, 3$, and 4 .

64 elements	Non- p -adaptivity	$k_{high} = 4$	Ratio
$t = 0.1$	1.70	0.50	3.40
$t = 0.2$	3.62	1.05	3.45
$t = 0.3$	5.53	2.15	2.57
$t = 0.4$	7.45	3.48	2.02
$t = 0.5$	9.37	5.27	1.78
256 elements	Non- p -adaptivity	$k_{high} = 4$	Ratio
$t = 0.1$	16.83	2.45	6.87
$t = 0.2$	35.10	6.53	5.38
$t = 0.3$	53.43	12.23	4.37
$t = 0.4$	71.78	19.58	3.67
$t = 0.5$	90.15	29.33	3.07

approximation are used in gray elements while low order $k_{low} = 1$ approximation are used in white elements. We will talk more about the efficiency of adaptivity at the end of this section.

In the next example, we show that the wavefronts are better reconstructed by high order schemes. In Fig. 4, the numerical simulations are done for order $k = 2, 3, 4$ and 5 respectively. The wavefronts start from a seed point at $(0, 0)$, propagate outward, and then reflect both from square boundary and the circular boundary which is glued by four piecewise parabola. We can clearly see that lower order schemes give wiggling solutions while high order schemes provide highly accurate solutions.

In Table 3, a qualitative comparison on the computational time for seed point at $(0, 0)$ and constant propagation speed $c(x) = 1$ in a square domain is given. In the p -adaptivity computation, we use piecewise linear approximation ($k_{low} = 1$) for low order elements and piecewise quintic approximation ($k_{high} = 4$) for high order elements. For coarse meshes, such as the one with 64 triangles, the method without p -adaptivity takes 1.78 times longer than the method with p -adaptivity for $k_{high} = 4$ at $t = 0.5$. The p -adaptivity computation does not gain too much mainly because the triangular elements are big in the coarse mesh which causes the wavefronts to touch most of elements. This means that we need to use higher degree polynomial approximations on most of elements. For finer meshes, like the one with 256 triangles, the method without p -adaptivity takes 3.07 times longer than the method with p -adaptivity for $k_{high} = 4$ at $t = 0.5$. This illustrated the efficiency in finer meshes. However, as time goes on, we notice that the time ratio drops no matter how fine is the

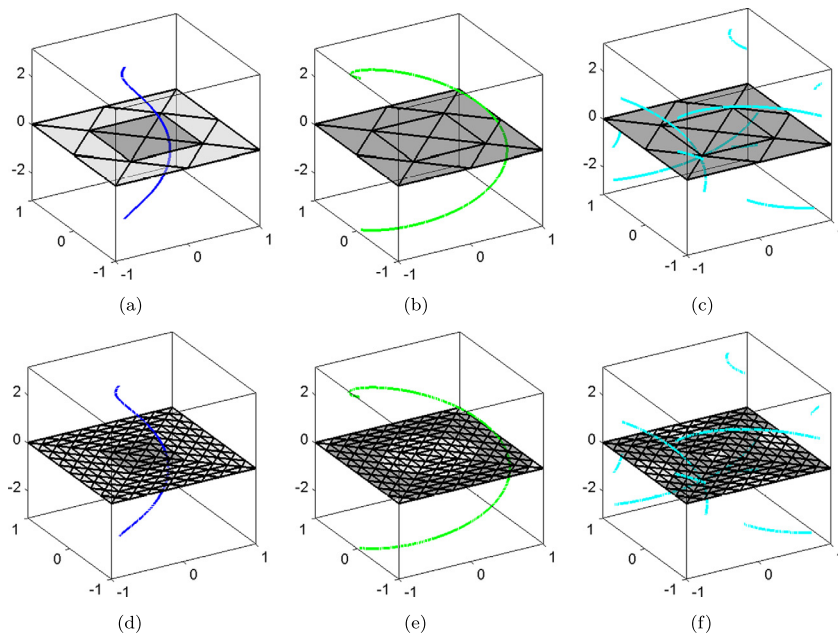


Fig. 5. p -Adaptivity on two different meshes with 16 and 256 elements at $t = 0.325$, $t = 0.975$ and $t = 1.625$ respectively. Elements with high order approximation are shown in dark gray color.

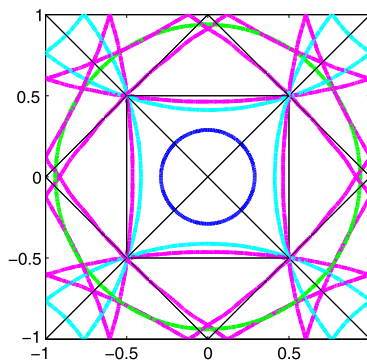


Fig. 6. The wavefronts at $t = 0.325$, $t = 0.975$, $t = 1.625$ and $t = 3.575$. We can clearly see that the wavefront will expand more and more elements as time goes on.

mesh. This is mainly because the surfaces in the phase space gets more convoluted and the wavefronts “expand” more and more elements. In particular, if the wavefronts keeps reflecting from the boundary, the wavefronts is going to “expand” all elements eventually.

In Fig. 5, we demonstrate the numerical results for two different meshes with 16 and 256 elements respectively. In the p -adaptivity computation, we use piecewise linear approximation ($k_{low} = 1$) for low order elements and piecewise quartic approximation ($k_{high} = 4$) for high order elements. The wavefronts in phase space at $t = 0.325$, $t = 0.975$, $t = 1.625$ for 16 elements are shown in (a), (b) and (c) and for 256 elements are shown in (d), (e) and (f) respectively. This confirms our argument that the wavefronts expand most of elements at a later time and also on a coarse mesh. The projection onto the physical space is shown in Fig. 6 on 16-element mesh. The wavefront at a much later time $t = 3.575$ shows the complexity of reflecting wavefronts.

5. Conclusion

We have presented a novel implementation of a recently introduced methodology for the simulation of high-frequency waves. The schemes are based on level-set formulations of the eikonal model which are discretized spectrally in the phase variables and with a discontinuous Galerkin procedure in physical space. The new approach incorporates an accurate treatment of interfaces through the use of isoparametric elements, and is accelerated with an adaptive strategy that relies on the use of high-order approximations only in a neighborhood of the wavefront in phase space. A variety of numerical examples demonstrate the improved capabilities that result from these amendments. In particular, we have shown that the use of

curved elements constitutes an actual *requirement* for the attainment of accurate solutions in the presence of non-flat (e.g. reflecting) boundaries, and that adaptive mechanisms can be used to achieve a significant computational speed-up without any sacrifice in accuracy. These developments suggest a number of directions for further improvement, including the derivation and use of a-posteriori error estimates (to provide further guidance in space-adaptivity), the adoption of alternative bases to represent phase variations (e.g. wavelets, to allow for localization) and the use of non-uniform time integrators (to weaken stability demands), which will be the subject of forthcoming work.

Acknowledgements

C.Y.K. would like to thank Ming-Huang Chen for fruitful discussions. C.Y.K. is partial supported by NSF DMS-1318364. F.R. gratefully acknowledges support from NSF through grant No. DMS-0311763.

Appendix A. Spatial basis functions and quadrature rules

In this appendix, and for the sake of completeness, we describe the spatial basis functions and quadratures that we use in the solution of (16). With regards to the former, we choose to work with a basis that results from consideration of a family of orthonormal polynomials of degree at most k on the reference triangle K_{ref} . The resulting diagonal nature of the mass matrices (13) corresponding to (flat) interior triangles makes this choice beneficial, even if this property is lost for the (curved) boundary elements. Specifically, the basis we considered [19] is constructed as an appropriate tensor product of the Jacobi polynomials $P_n^{\alpha,\beta}(x)$ which are defined by

$$\begin{aligned}
 P_0^{\alpha,\beta}(x) &= 1, \\
 P_1^{\alpha,\beta}(x) &= \frac{1}{2}(\alpha - \beta + (\alpha + \beta + 2)x), \\
 2(n + 1)(n + \alpha + \beta + 1)(2n + \alpha + \beta)P_{n+1}^{\alpha,\beta}(x) \\
 &= \left\{ (2n + \alpha + \beta + 1)(\alpha^2 - \beta^2) + x \frac{(2n + \alpha + \beta + 2)!}{(2n + \alpha + \beta - 1)!} \right\} P_n^{\alpha,\beta} - 2(n + \alpha)(n + \beta)(2n + \alpha + \beta + 2)P_{n-1}^{\alpha,\beta}
 \end{aligned}$$

or

$$P_n^{\alpha,\beta}(x) = \frac{1}{(-1)^n 2^n n! (1-x)^\alpha (1+x)^\beta} \frac{d^n}{dx^n} \{ (1-x)^\alpha (1+x)^\beta (1-x^2)^n \}.$$

An orthonormal basis on $K_{ref} = \{(r, s) \in [-1, 1] \times [-1, 1], r + s \leq 1\}$ then is given by

$$\phi_i(r, s) = \phi_{(nm)}(r, s) = P_n^{0,0}(a) \left(\frac{1-b}{2} \right)^n P_m^{2n+1,0}(b) / \sqrt{\left(\frac{2}{2n+1} \right) \left(\frac{1}{n+m+1} \right)}$$

where

$$i = \frac{1}{2}(n + m + 1)(n + m + 2) - n, \quad a = \frac{2(1+r)}{(1-s)} - 1 \quad \text{and} \quad b = s.$$

From the orthogonality relation

$$\int_{-1}^1 \left(\frac{1-x}{2} \right)^\alpha \left(\frac{1-y}{2} \right)^\beta P_n^{\alpha,\beta}(x) P_m^{\alpha,\beta}(x) dx = \delta_{nm} \frac{2}{2n + \alpha + \beta + 1} \frac{(n + \alpha)!(n + \beta)!}{n!(n + \alpha + \beta)!}$$

it readily follows that

$$\int_{-1}^{-1-s} \int_{-1}^{-1-s} \phi_{(nm)} \phi_{(n'm')} dr ds = \delta_{nn'} \delta_{mm'}.$$

Also, the evaluation of the integrals in (14), (15) require the calculation of the partial derivatives of ϕ_i . In this connection, we have

$$\frac{\partial \phi_i(r, s)}{\partial r} = \left(\frac{2}{1-s} \right) \frac{dP_n^{0,0}(a)}{da} \left(\frac{1-b}{2} \right)^n P_m^{2n+1,0}(b) / \sqrt{\left(\frac{2}{2n+1} \right) \left(\frac{1}{n+m+1} \right)}$$

and, using the identity

$$\frac{dp_n^{\alpha,\beta}(a)}{da} = \left(\frac{n+\alpha+\beta+1}{2}\right) p_{n-1}^{\alpha+1,\beta+1}(a),$$

we obtain

$$\frac{\partial\phi_i(r,s)}{\partial r} = \begin{cases} \left(\frac{n+1}{2}\right) p_{n-1}^{1,1}\left(\frac{2(1+r)}{1-s} - 1\right) \left(\frac{1-s}{2}\right)^{n-1} P_m^{2n+1,0}(s) / \sqrt{\left(\frac{2}{2n+1}\right)\left(\frac{1}{n+m+1}\right)} & \text{when } n \geq 1, \\ 0 & \text{when } n = 0. \end{cases}$$

Similarly, the s -derivative is given by

$$\begin{aligned} \frac{\partial\phi_i(r,s)}{\partial s} &= \frac{2(1+r)}{(1-s)^2} \left(\frac{n+1}{2}\right) p_{n-1}^{1,1}\left(\frac{2(1+r)}{1-s} - 1\right) \left(\frac{1-s}{2}\right)^n P_m^{2n+1,0}(s) / \sqrt{\left(\frac{2}{2n+1}\right)\left(\frac{1}{n+m+1}\right)} \\ &\quad - p_n^{0,0} \left(\frac{2(1+r)}{1-s} - 1\right) \frac{n}{2} \left(\frac{1-s}{2}\right)^{n-1} P_m^{2n+1,0}(s) / \sqrt{\left(\frac{2}{2n+1}\right)\left(\frac{1}{n+m+1}\right)} \\ &\quad + p_n^{0,0} \left(\frac{2(1+r)}{1-s} - 1\right) \left(\frac{1-s}{2}\right)^n \left(\frac{m+2n+2}{2}\right) P_{m-1}^{2n+2,1}(s) / \sqrt{\left(\frac{2}{2n+1}\right)\left(\frac{1}{n+m+1}\right)}. \end{aligned}$$

Finally, we consider the issue of approximation of the two-dimensional integrals on K_{ref} triangle in (14), (15) and of the line (edge) integrals in (16). For two dimensional integrals, we use symmetric quadrature rules proposed by Wandzura [24]. The method uses a simple group theory and numerical optimization to design the quadrature rules up to order 30 on the equilateral triangle T_{eq} with the vertices $(1, 0)$, $(-\frac{1}{2}, \frac{\sqrt{3}}{2})$ and $(-\frac{1}{2}, -\frac{\sqrt{3}}{2})$. Basically, the form

$$\sum_{i=1}^n w_i f(x_i, y_i)$$

serves to approximate the integral

$$\int_{T_{eq}} f(x, y) dx dy$$

up to a certain order accuracy by choosing the weights w_i and quadrature points (x_i, y_i) appropriately. These weights w_i and quadrature points (x_i, y_i) are given in the paper. Since we now want to compute the integral on the reference triangles T_{ref} with the vertices $(1, -1)$, $(-1, 1)$ and $(-1, -1)$, we use the linear transformation

$$\begin{aligned} \tilde{x} &= \frac{4}{3}x - \frac{1}{3}, \\ \tilde{y} &= -\frac{2}{3}x + \frac{2}{\sqrt{3}}y - \frac{1}{3} \end{aligned}$$

to get the quadrature points $(\tilde{x}_i, \tilde{y}_i)$ on the reference triangle T_{ref} and $\tilde{w}_i = \frac{8}{3\sqrt{3}} w_i$. For the line integral, we simply use the Gaussian quadrature rule [23].

References

- [1] D. Andersh, J. Moore, S. Kosanovich, D. Kapp, R. Bhalla, R. Kipp, T. Courtney, A. Nolan, F. German, J. Cook, J. Hughes, Xpatch 4: The next generation in high frequency electromagnetic modeling and simulation software, in: IEEE National Radar Conference, 2000, pp. 844–849.
- [2] S. Bartels, C. Carstensen, A. Hecht, P2q2iso2d = 2d isoparametric fem in matlab, J. Comput. Appl. Math. 192 (2006) 219–250.
- [3] F. Bassi, S. Rebay, High-order accurate discontinuous finite element solution of the 2d Euler equations, J. Comput. Phys. 138 (1997) 251–285.
- [4] K.J. Bathe, Finite Element Procedures, Prentice-Hall, Upper Saddle River, NJ, 1995.
- [5] M.-H. Chen, B. Cockburn, F. Reitich, High-order rkdg methods for computational electromagnetics, J. Sci. Comput. 22 (2005) 205–226.
- [6] L.-T. Cheng, H. Liu, S. Osher, Computational high-frequency wave propagation using the level-set method with applications to the semi-classical limit of the Schrödinger equations, Commun. Math. Sci. 1 (3) (2003) 593–621.
- [7] B. Cockburn, J. Qian, F. Reitich, J. Wang, An accurate spectral/discontinuous finite-element formulation of a phase-space-based level set approach to geometrical optics, J. Comput. Phys. 208 (2005) 175–195.
- [8] B. Cockburn, C.-W. Shu, The Runge–Kutta discontinuous Galerkin finite element method for conservation laws V: Multidimensional systems, J. Comput. Phys. 141 (1998) 199–224.
- [9] M.G. Crandall, P.L. Lions, Two approximations of solutions of Hamilton–Jacobi equations, Math. Comput. 43 (1984) 1–19.
- [10] Michael G. Crandall, Hitoshi Ishii, Pierre-Louis Lions, User's guide to viscosity solutions of second order partial differential equations, Bull., New Ser., Am. Math. Soc. 27 (1) (1992) 1–67.
- [11] B. Engquist, O. Runborg, Computational high frequency wave propagation, Acta Numer. 1 (2003) 181–266.
- [12] S. Gottlieb, C.-W. Shu, E. Tadmor, Stong stability preserving high order time discretization methods, SIAM Rev. 43 (2000) 89–112.
- [13] S. Jin, S. Osher, A level set method for the computation of multivalued solutions to quasi-linear hyperbolic PDEs and Hamilton–Jacobi equations, Commun. Math. Sci. 1 (3) (2003) 575–591.

- [14] H. Liu, L.-T. Cheng, S. Osher, A level set framework for capturing multi-valued solutions of nonlinear first-order equations, *J. Sci. Comput.* 29 (3) (2006) 353–373.
- [15] S. Operto, S. Xu, G. Lambare, Can we image quantitatively complex models with rays?, *Geophysics* 65 (2000) 1223–1238.
- [16] S. Osher, L.-T. Cheng, M. Kang, H. Shim, Y.-H. Tsai, Geometric optics in a phase-space-based level set and Eulerian framework, *J. Comput. Phys.* 179 (2002) 622–648.
- [17] J. Qian, L.-T. Cheng, S. Osher, A level set-based Eulerian approach for anisotropic wave propagation, *Wave Motion* 37 (4) (2003) 365–379.
- [18] F. Reitich, K.K. Tamma, State-of-the-art, trends and directions in computational electromagnetics, *Comput. Model. Eng. Sci.* 5 (2004) 287–294.
- [19] S.J. Sherwin, G.E. Karniadakis, A new triangular and tetrahedral basis for high-order (hp) finite element methods, *Int. J. Numer. Methods Eng.* 38 (22) (1995) 3775–3802.
- [20] V. Vinje, E. Iversen, K. Astebol, H. Gjøystdal, Estimation of multivalued arrivals in 3D models using wavefront construction, Part I, *Geophys. Prospect.* 44 (1996) 819–842.
- [21] V. Vinje, E. Iversen, K. Astebol, H. Gjøystdal, Estimation of multivalued arrivals in 3D models using wavefront construction, Part II: Tracing and interpolation, *Geophys. Prospect.* 44 (1996) 843–858.
- [22] V. Vinje, E. Iversen, H. Gjøystdal, Traveltime and amplitude estimation using wavefront construction, *Geophysics* 58 (8) (1993) 1157–1166.
- [23] B.P. Flannery, W.H. Press, S.A. Teukolsky, *Numerical Recipes in C*, Cambridge University Press, 1988.
- [24] S. Wandzura, Symmetric quadrature rules on a triangle, *Comput. Math. Appl.* 45 (2003) 1829–1840.
- [25] G.B. Whitham, *Linear and Nonlinear Waves*, Wiley, 1974.